Submitted to ADVANCED OPTICAL MATERIALS

DOI: 10.1002/(adom.201700277R1)
Article type: Communication

Polarization and frequency multiplexed terahertz meta-holography

Qiu Wang, Xueqian Zhang, Prof. Eric Plum, Quan Xu, Minggui Wei, Yuehong Xu, Huifang Zhang, Yi Liao, Prof. Jianqiang Gu, Prof. Jiaguang Han, Prof. Weili Zhang**

Q. Wang, X. Zhang, Q. Xu, M. Wei, Y. Xu, H. Zhang, Prof. J. Gu, Prof. J. Han, and Prof. W. Zhang
Center for Terahertz Waves and College of Precision Instrument and Optoelectronics Engineering
Tianjin University
Tianjin 300072, People's Republic of China
E-mail: jiaghan@tju.edu.cn

Prof. E. Plum
Optoelectronics Research Centre and Centre for Photonic Metamaterials
University of Southampton
Highfield, Southampton, SO17 1BJ, UK

Y. Liao
School of Science
Tianjin University
Tianjin 300072, People's Republic of China

Prof. W. Zhang
School of Electrical and Computer Engineering
Oklahoma State University
Stillwater, Oklahoma 74078, USA
E-mail: weili.zhang@oktate.edu

Keywords: Meta-holography, Polarization-frequency multiplexed, Phase-amplitude modulation

There are four fundamental characteristics of electromagnetic waves: phase, amplitude, polarization, and frequency. Precise control over these properties of electromagnetic waves and their spatial distribution has always been underpinning progress in optics. Metasurfaces, also known as planar metamaterials, have aroused explosive attention recently due to their capability of tailoring the phase and amplitude distribution of outgoing electromagnetic waves as desired.[1-5] Numerous intriguing effects and applications based on metasurfaces have been discovered, including anomalous reflection and refraction,[6-8] special beams generation,[9-12] wave plates,[13,14] ultrathin flat lenses,[15-17] and cloaking.[18,19] In particular, metasurface based holography, namely meta-holography, has been demonstrated with plasmonic or dielectric subwavelength unit cells[20-32] and metallic hole or groove patterns.[33-35] By allowing simultaneous control of amplitude and phase in each pixel,[5,27] metasurfaces offer a new degree of freedom compared to conventional structures and devices, which is especially significant in holography. Besides, with subwavelength pixel sizes and unlimited pixel numbers, high-resolution holograms and complex hybrid holography have been demonstrated.[20-32]

In this article, we propose and demonstrate a polarization and frequency multiplexed meta-hologram with simultaneous amplitude and phase modulation in every pixel. Thus, we engineer the meta-hologram with respect to all four fundamental properties of electromagnetic waves, including polarization, frequency, amplitude and phase. By utilizing C-shape bar resonators (CBRs) as the basic pixels, simultaneous amplitude and phase modulation on the hologram can be achieved. Fiber-based near-field scanning terahertz microscopy is applied for experimental characterization due to its high resolution and high scanning speed. The respective holographic images of “C”, “F”, “T”, and “W” at different frequencies and different polarizations are demonstrated theoretically and experimentally. The proposed polarization and frequency selective meta-hologram provides a novel

holographic design approach and may have potential applications in frequency, polarization and space division multiplexing systems.

Choosing the functional structures of subwavelength size that determine the properties of each effective pixel is of great significance in the design process. To realize polarization-selective and frequency-selective properties, each pixel is divided into four subpixels, as shown in **Figure 1**. C-shape split ring resonators have been demonstrated to be capable of simultaneously manipulating the phase and amplitude of every pixel with large bandwidth.[5,27] However, to restrain the response overlap between the subpixels, good monochromaticity for the subpixels is required here. CBRs whose opening angles are larger than C-shape split ring resonators are employed as the basic subpixels. The CBRs are made from 200-nm-thick aluminum and patterned on a 500-μm-thick high-resistivity silicon substrate. Like for C-shape split ring resonators, when the CBR rotates around the *z*-axis, the phase shift of outgoing *y*-polarized component remains constant under *x*-polarized illumination, except for a π jump when the symmetry axis passes the *x*-axis. Meanwhile, the amplitude of *y*-polarized component E_y follows

$$\left|E_y\right| \propto \left|\sin(2\beta)\right| \tag{1}$$

where β represents the orientation of the CBR's symmetry axis relative to the *x*-axis.[5,27] Besides, CBRs have better monochromaticity, making them more suitable for our design. Through numerical simulation using a commercial software, CST Microwave Studio, two CBRs are selected with geometric parameters of (r, w, θ) = (28 μm, 5 μm, 77°) and (32 μm, 10 μm, 115°), which work at 0.6 and 0.8 THz respectively. Their simulated intensity transmissions of the *y*-polarized component $|E_y|^2$ are given in Figure 1, when the incident plane wave is *x*-polarized. In this situation, units 1 and 2 contribute to E_y at 0.6 and 0.8 THz respectively, while units 3 and 4 cannot generate *y*-polarized radiation as their symmetry axis

is aligned with the incident polarization. And when the incident polarization is rotated by 45° clockwise or anticlockwise, units 3 and 4 are "turned on", while units 1 and 2 are "turned off". Units 1 and 4 (highlighted blue) mainly contribute at 0.6 THz and units 2 and 3 (highlighted red) mainly contribute at 0.8 THz. Thus, the independent manipulation of two polarizations and two frequencies has been achieved. The size of each subpixel is 100 μm × 100 μm, so size of a whole pixel of the meta-hologram is 200 μm × 200 μm.

To design the polarization and frequency selective meta-hologram, the Rayleigh-Sommerfeld diffraction theory is applied to calculate the electric field amplitude and phase distribution in the hologram. The designed image plane is located 5 mm away from the meta-hologram. The meta-hologram has an overall size of 2 cm × 2 cm, containing 100 × 100 pixels. After normalization and linear approximation, two-level amplitude modulation (0 or 1) and two-level phase modulation (0 or π) on each subpixel of every pixel are adopted in the meta-hologram. The two-level amplitude modulation is achieved by whether there's a CBR or not on that subpixel. And the two-level phase modulation is achieved by simply rotating the CBR on that subpixel by 90° so that the phase shift changes by π while the amplitude remains constant, see **Equation 1**. Holographic images of "C", "F", "T", or "W" are expected at 0.6 and 0.8 THz for two different polarizations, as illustrated by **Figure 2**. To simplify the experiment, the polarization-selectivity is measured by rotating the meta-hologram, while keeping the incident and detected polarization directions fixed.

The numerically calculated electric field intensity distributions $|E_y|^2$ on the designed holographic image plane at z = 5 mm are shown in **Figure 3**a-d. All the four letters are designed with the same image plane to simplify the measurement, however, each image could also be designed with an independent image plane actually. The calculation is based on Rayleigh-Sommerfeld diffraction theory, taking the response overlap between different sub-pixels into account by employing the data shown in Figure 1. Good, clear holographic images

of the four letters are predicted at the two different polarizations and two different frequencies, respectively.

The proposed meta-hologram is fabricated by conventional photolithography. Interpolated measurements of the *y*-polarized electric field intensity distributions on the *xy*-plane at z = 5 mm by fiber-based near-field scanning terahertz microscopy are shown in Figure 3e-h. As expected, the holographic images of "C" and "F" appear at 0.6 and 0.8 THz, respectively, and when the meta-hologram is rotated by 45° around the *z*-axis, the holographic images change into "T" and "W" at 0.6 and 0.8 THz respectively. The simulated and experimental results are in good agreement for both polarizations and both frequencies, including the image sizes, profiles, locations, and relative intensity distributions, demonstrating the good holographic imaging characteristics of the meta-hologram. The reduced experimental signal to noise ratio (SNR) is mainly due to imperfect alignment of the electric field detection orientation with the *y*-axis and the experimental scanning resolution. The electric field is detected at 0.5 mm intervals from -10 mm to 10 mm in both the *x* and *y* directions (only 41×41 samples) and then solved by interpolation, leading to relatively low resolution of the experimental results, especially nearby the image edges. However, it will be time-consuming and difficult to employ smaller detection intervals in our experimental situation, as scanning detection is adopted in the *xy*-plane, which is quite different from the charge coupled device (CCD) detection method used in the visible regime. Besides, the present meta-hologram employs only two-level amplitude modulation and two-level phase modulation. The holographic image quality can be further optimized by employing more-level amplitude and phase modulation, which however, is extremely difficult to achieve in our polarization and frequency multiplexing design situation. The crosstalk between CBRs that are intended for the two different frequencies is small, providing high contrast between

frequency-selected holograms. We do not observe any twin image effect or zero-order spot, from which conventional holograms usually suffer.

The evolution of the holographic images during rotation of the meta-hologram is illustrated in **Figure 4**. While the meta-hologram rotates from $\alpha = 0°$ to $\alpha = 45°$, the measured holographic image of "C" disappears and the image of "T" emerges gradually at 0.6 THz. The disappearance of "F" and emergence of "W" can be observed at 0.8 THz. The change in intensity of holographic images with α is not linear but proportional to $\sin^2(2\alpha)$ as illustrated by Equation 1. The image of "C" will reappear and "T" will disappear again when α is increased further from 45° to 90°. As disappearance and reappearance of the holographic images is periodic with meta-hologram rotation, repeating every 90°, each letter appears and disappears four times during a full rotation of the meta-hologram. Such 90° periodicity of optical properties with rotation is rare in conventional optics. These results show that the meta-hologram offers a flexible design method for metasurfaces that provide independent functionalities for electromagnetic signals with different frequency, polarization or spatial distribution.

By adopting a partitioning approach, a polarization and frequency multiplexed meta-hologram is demonstrated. However, our current realization of frequency and polarization multiplexed meta-holography suffers from low efficiency. Taking holographic image of "C" as an example, the diffraction efficiency (DE) is defined as the ratio between the sum of output *y*-polarized electric field intensity in the target "C" region and the sum of all the input electric field intensity. The measured DE is 0.22 %, 0.17 %, 0.16 %, and 0.26 % for "C", "F", "T", and "W" at different frequencies and different polarizations, respectively. The relatively low DE is mainly due to the partitioning design and the low cross-polarization conversion efficiency by employing the single-layer, transmission-type, plasmonic metasurface. The cross-polarization conversion efficiency could be significantly improved by adopting multi-

layer structures,[36] reflective structures,[24] or dielectric metamaterials,[29] all of which are compatible with the partitioning approach presented here.

In summary, we present a polarization and frequency selective meta-hologram. Simultaneous and independent binary control of both amplitude and phase of electromagnetic fields of different polarizations and frequencies is achieved in every pixel on the hologram. Thus, the meta-hologram makes use of all four fundamental properties of electromagnetic waves – phase, amplitude, polarization and frequency – to store holographic images of characters "C", "F", "T", and "W" at different frequencies and different polarizations. The unique meta-holography approach demonstrated here delivers new flexibility in manipulating electromagnetic waves and a new path to realize metasurfaces with different functionalities for radiations of different frequencies, polarizations or spatial distributions. Such multi-channel meta-holograms can store multiple sets of information as well as transform and redirect multiple optical signals in different ways, therefore would find applications in optical data storage and communications, e.g. in polarization, wavelength and space division multiplexing.

Experimental Section

Fiber-based near-field scanning terahertz microscopy is employed experimentally to detect the different holographic images, as shown in **Figure 5**. Femtosecond fiber laser pulses with ~50 fs pulse width and 1550 nm central wavelength are split into two beams. One of the beams focuses onto a commercial photoconductive antenna to generate broadband terahertz radiation ranging from 0.2 to 1.5 THz. The other beam, with transformation into free space and then second harmonic generation in lithium niobate (PPLN), illuminates a commercial terahertz near-field probe to detect the outgoing terahertz waves with high resolution. A terahertz polarizer is placed before the metasurface to ensure the incident beam is precisely *x*-

polarized, while the antenna gap of the terahertz probe is set along the perpendicular orientation to detect only the *y*-polarized electric field component. To characterize the holographic images of "C" and "F" on the image plane (z = 5 mm), the electric field is detected with 0.5 mm steps from -1 cm to 1 cm in both x and y directions. To detect the holographic exhibitions of "T" and "W", the hologram is rotated by 45° around the z-axis first and then the electric field is detected by the identical scan process.

The proposed meta-hologram is fabricated by conventional photolithography. A layer of photoresist (AZ P4000) is first spin-coated on the slicon substrate; then, the CBR patterns are exposed with standard lithography; after development, the sample is deposited with a 200-nm-thick Al by using thermal evaporation; the photoresist and Al outside the structural area are removed by lift-off process. The partial optical microscope image of the fabricated meta-hologram is shown in Figure 5b. The "missing" SBR in the top left corner of Figure 5b represents that the amplitude of that subpixel is zero. The fabrication quality can be seen more clearly in a magnified optical microscope image of a single CBR, as shown in Figure 5c.

Acknowledgements

This work was supported by the National Natural Science Foundation of China (Grant Nos. 61422509, 61307125, 61427814, 61420106006, and 61328503), the National Key Basic Research Special Foundation of China (Grant No. 2014CB339800), the Program for Changjiang Scholars and Innovative Research Team in Universities (Grant No. IRT13033), the U. S. National Science Foundation (Grant No. ECCS-1232081), and the UK's Engineering and Physical Sciences Research Council (Grant No. EP/M009122/1).

Received:
Revised:
Published online:

[1] A. V. Kildishev, A. Boltasseva, V. M. Shalaev, *Science* **2013**, *339*, 1232009.

[2] N. Meinzer, W. L. Barnes, I. R. Hooper, *Nat. Photonics* **2014**, *8*, 889.

[3] N. Yu, F. Capasso, *Nat. Mater.* **2014**, *13*, 139.

[4] N. M. Estakhri, A. Alù, *J. Opt. Soc. Am. B* **2016**, *33*, A21.

[5] L. Liu, X. Zhang, M. Kenney, X. Su, C. Ouyang, Y. Shi, J. Han, W. Zhang, S. Zhang, *Adv. Mater.* **2014**, *26*, 5031.

[6] N. K. Grady, J. E. Heyes, D. R. Chowdhury, Y. Zeng, M. T. Reiten, A. K. Azad, A. J. Taylor, D. A. R. Dalvit, H. T. Chen, *Science* **2013**, *340*, 1304.

[7] X. Zhang, Z. Tian, W. Yue, J. Gu, S. Zhang, J. Han, W. Zhang, *Adv. Mater.* **2013**, *25*, 4567.

[8] J. Shi, X. Fang, E. T. F. Rogers, E. Plum, K. F. MacDonald, N. I. Zheludev, *Opt. Express* **2014**, *22*, 21051.

[9] N. Yu, P. Genevet, M. A. Kats, F. Aieta, J. P. Tetienne, F. Capasso, Z. Gaburro, *Science* **2011**, *334*, 333.

[10] Y. Yang, W. Wang, P. Moitra, I. I. Kravchenko, D. P. Briggs, J. Valentine, *Nano lett.* **2014**, *14*, 1394.

[11] L. Li, T. Li, S. M. Wang, C. Zhang, S. N. Zhu, *Phys. Rev. Lett.* **2011**, *107*, 126804.

[12] L. Li, T. Li, S. M. Wang, S. N. Zhu, *Phys. Rev. Lett.* **2013**, *110*, 046807.

[13] T. Guo, C. Argyropoulos, *Opt. Lett.* **2016**, *41*, 5592.

[14] L. Cong, N. Xu, J. Gu, R. Singh, J. Han, W. Zhang, *Laser & Photonics Rev.* **2014**, *8*, 626.

[15] F. Aieta, P. Genevet, M. A. Kats, N. Yu, R. Blanchard, Z. Gaburro, F. Capasso, *Nano Lett.* **2012**, *12*, 4932.

[16] X. Jiang, J. Ye, J. He, X. Wang, D. Hu, S. Feng, Q. Kan, Y. Zhang, *Opt. Express* **2013**, *21*, 30030.

[17] Q. Wang, X. Zhang, Y. Xu, Z. Tian, J. Gu, W. Yue, S. Zhang, J. Han, W. Zhang, *Adv. Optical Mater.* **2015**, *3*, 779.

[18] X. Ni, Z. J. Wong, M. Mrejen, Y. Wang, X. Zhang, *Science* **2015**, *349*, 1310.

[19] B. Orazbayev, N. M. Estakhri, A. Alù, M. Beruete, *Adv. Optical Mater.* **2016**, *5*, 1600606.

[20] X. Ni, A. V. Kildishev, V. M. Shalaev, *Nat. Commun*. **2013**, *4*, 2807.

[21] L. Huang, X. Chen, H. Mühlenbernd, H. Zhang, S. Chen, B. Bai, Q. Tan, G. Jin, K. Cheah, C. Qiu, J. Li, T. Zentgraf, S. Zhang, *Nat. Commun*. **2013**, *4*, 2808.

[22] W. T. Chen, K. Y. Yang, C. M. Wang, Y. W. Huang, G. Sun, I. D. Chiang, C. Y. Liao,

W. L. Hsu, H. T. Lin, S. Sun, L. Zhou, A. Q. Liu, D. P. Tsai, *Nano Lett*. **2014**, *14*, 225.

[23] Y. W. Huang, W. T. Chen, W. Y. Tsai, P. C. Wu, C. M. Wang, G. Sun, D. P. Tsai, *Nano Lett.* **2015**, *15*, 3122.

[24] G. Zheng, H. Mühlenbernd, M. Kenney, G. Li, T. Zentgraf, S. Zhang, *Nat. Nanotechnol*. **2015**, *10*, 308.

[25] P. Genevet, F. Capasso, *Rep. Prog. Phys*. **2015**, *78*, 024401.

[26] L. Huang, H. Mühlenbernd, X. Li, X. Song, B. Bai, Y. Wang, T. Zentgraf, *Adv. Mater.* **2015**, *27*, 6444.

[27] Q. Wang, X. Zhang, Y. Xu, J. Gu, Y. Li, Z. Tian, R. Singh, S. Zhang, J. Han, W. Zhang, *Sci. Rep.* **2016**, *6*, 32867.

[28] X. Li, L. Chen, Y. Li, X. Zhang, M. Pu, Z. Zhao, X. Ma, Y. Wang, M. Hong, X. Luo, *Sci. Adv.* **2016**, *2*, e1601102.

[29] M. Khorasaninejad, A. Ambrosio, P. Kanhaiya, F. Capasso, *Sci. Adv.* **2016**, *2*, e1501258.

[30] M. Papaioannou, E. Plum, J. Valente, E. T. F. Rogers, N. I. Zheludev, *Light: Sci. & Appl.* **2016**, *5*, e16070.

[31] W. Ye, F. Zeuner, X. Li, B. Reineke, S. He, C. W. Qiu, J. Liu, Y. Wang, S. Zhang, T. Zentgraf, *Nat. Commun.* **2016**, *7*, 11930.

[32] J. P. B. Mueller, N. A. Rubin, R. C. Devlin, B. Groever, F. Capasso, *Phys. Rev. Lett.* **2017**, *118*, 113901.

[33] Y. H. Chen, L. Huang, L. Gan, Z. Y. Li, *Light: Sci. & Appl.* **2012**, *1*, e26.

[34] Y. H. Chen, M. Zhang, L. Gan, X. Wu, L. Sun, J. Lin, J. Wang, Z. Y. Li, *Opt. Express* **2013**, *21*, 17558.

[35] P. Genevet, J. Lin, M. A. Kats, F. Capasso, *Nat. Commun*. **2012**, *3*, 1278.

[36] S. Liu, A. Noor, L. L. Du, L. Zhang, Q. Xu, K. Luan, T. Q. Wang, Z. Tian, W. X. Tang, J. G. Han, W. L. Zhang, X. Y. Zhou, Q. Cheng, T. J. Cui, *ACS Photonics* **2016**, *3*, 1968.

Figures with Captions

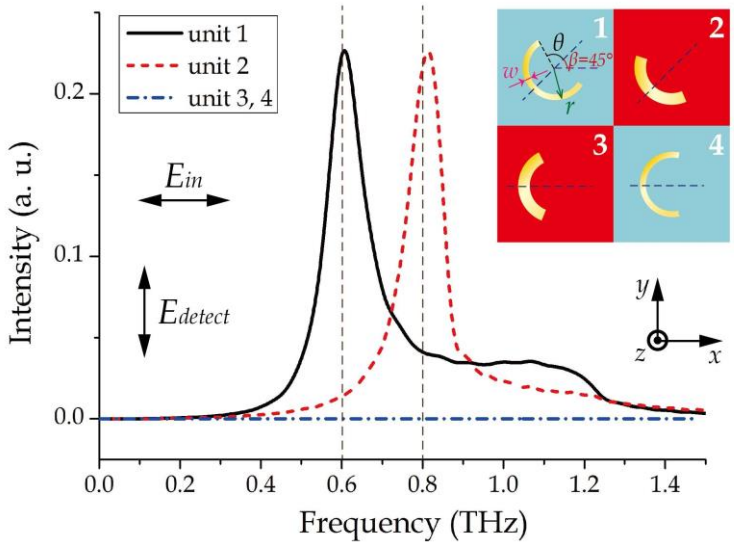

Figure 1. Illustration of the four basic functional subpixels and their simulated electric field responses. r, w, β, and 2θ represent outer radius, width, orientation angle with respect to the x-axis, and opening angle of the CBRs respectively. β is 45° for units 1 and 2, and is zero for units 3 and 4. The incident wave is x-polarized and the transmitted y-polarized electric field intensity $|E_y|^2$ is detected. The black solid line and the red dotted line represent the responses of unit 1 and unit 2, respectively. The responses of units 3 and 4 both equal zero, shown by the blue dash dot line.

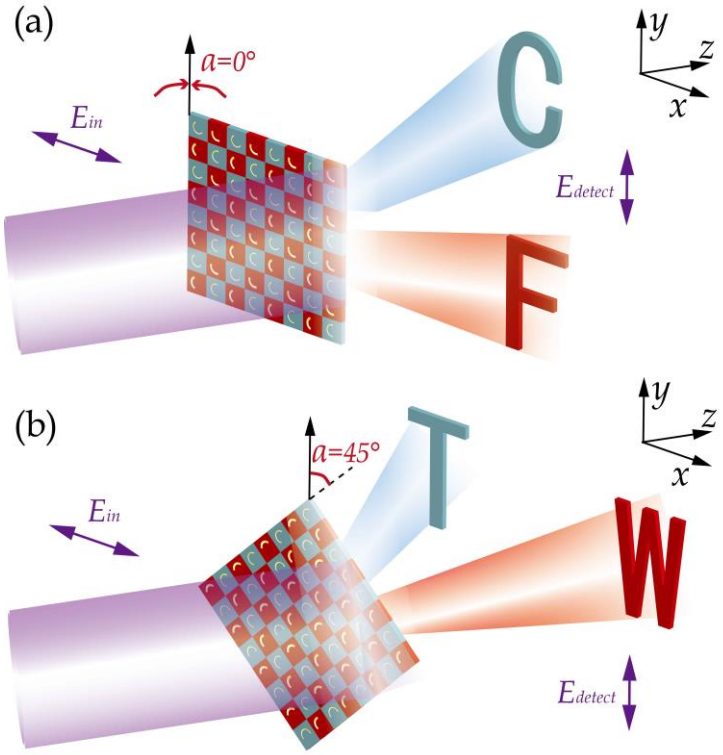

Figure 2. Schematic illustration of the polarization and frequency selective meta-hologram's functionality. a) Holographic images of "C" and "F" appear at 0.6 THz (blue) and 0.8 THz (red), respectively. b) Holographic images of "T" and "W" appear at 0.6 and 0.8 THz when the meta-hologram is rotated by 45° around the *z*-axis.

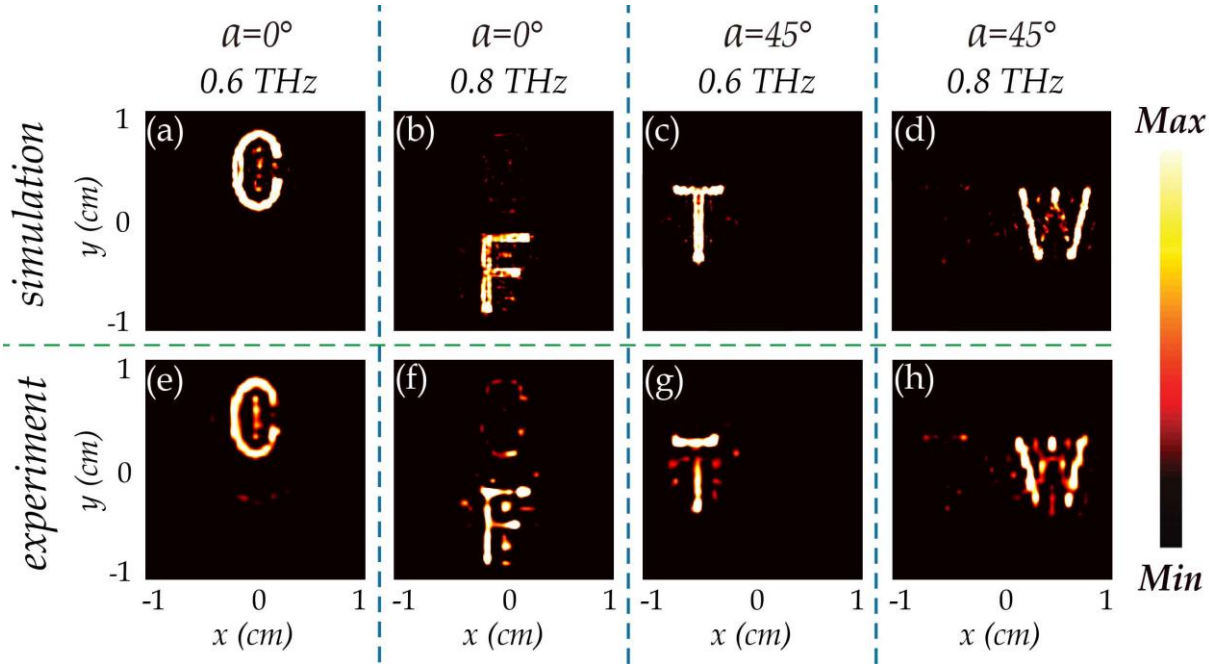

Figure 3. Holographic images of the polarization and frequency selective meta-hologram. The incident THz radiation is *x*-polarized. The images show the *y*-polarized electric field intensity distributions $|E_y|^2$ on the image plane for different metasurface orientations α and different THz frequencies. a-d) Numerically simulations. e-h) Measurements by fiber-based near-field scanning terahertz microscopy.

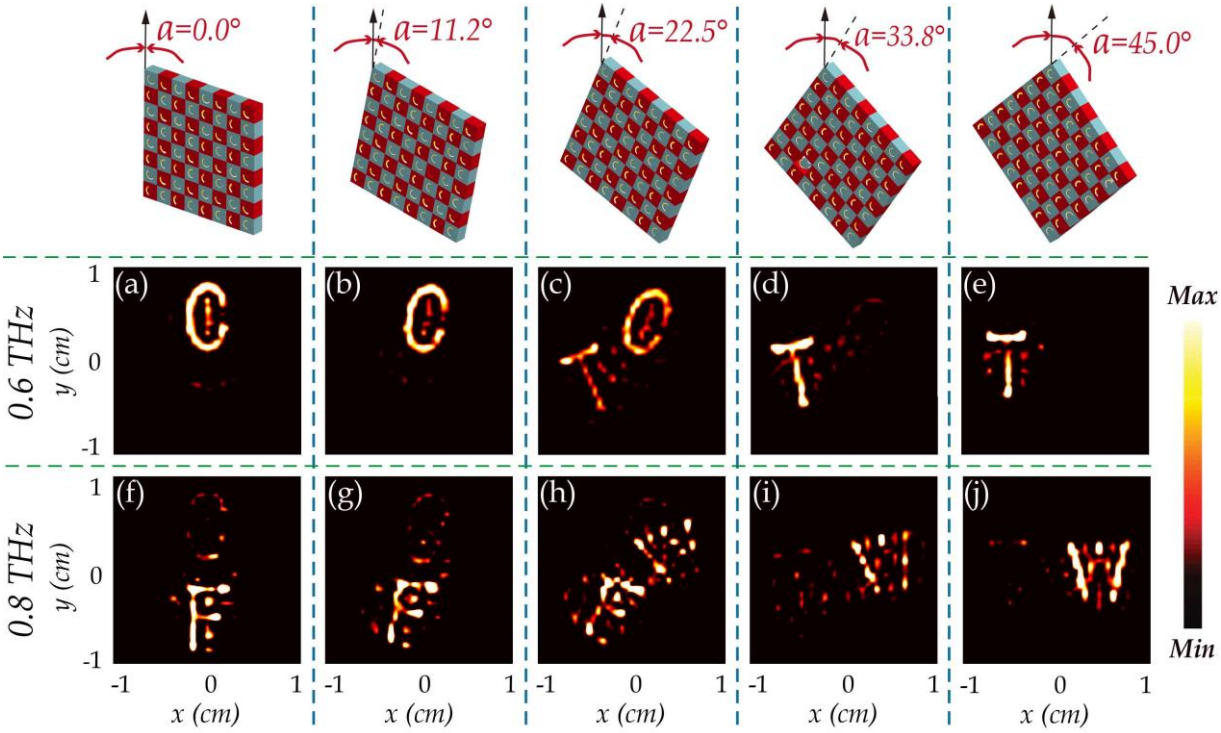

Figure 4. a-j) Evolution of the holographic images during meta-hologram rotation measured by fiber-based near-field scanning terahertz microscopy. The images show the measured *y*-polarized electric field intensity distribution on the image plane for different metasurface orientations α at frequencies of 0.6 THz and 0.8 THz, under *x*-polarized illumination.

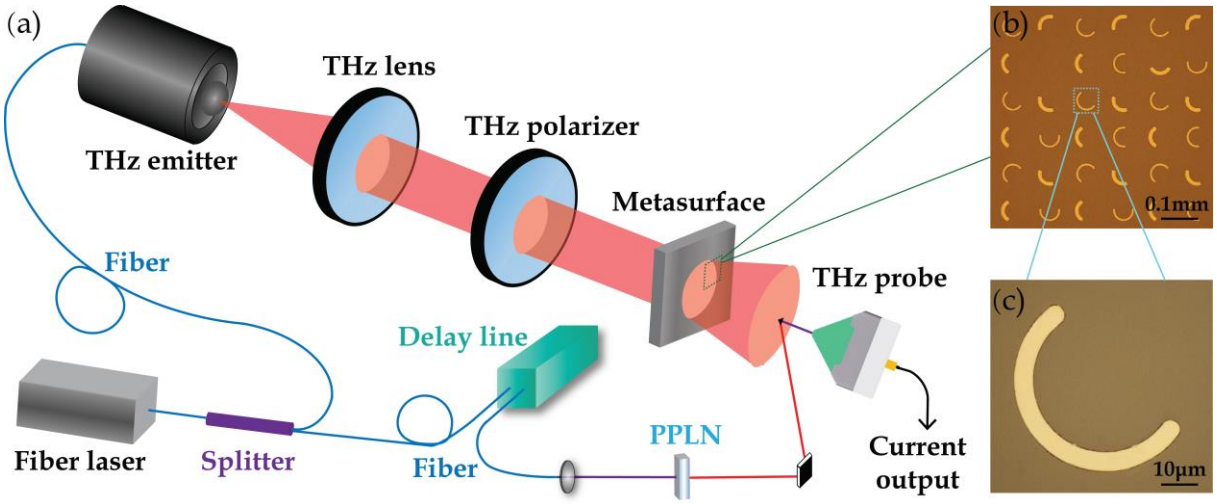

Figure 5. Illustration of the experimental setup. a) Schematic of fiber-based near-field scanning terahertz microscopy. A THz photoconductive antenna is employed as the THz emitter and a near-field terahertz probe is used to detect the THz signal. b) Partial optical microscope image of the meta-hologram. c) Magnified optical microscope image of a single CBR in the meta-hologram.

A Polarization and frequency multiplexed meta-hologram is reported. With polarization and frequency selective independent simultaneous control of amplitude and phase in every pixel, the meta-hologram makes use of all four fundamental properties of electromagnetic waves. Generation of holographic images of "C", "F", "T", or "W" depending on polarization and frequency is demonstrated theoretically and experimentally. Our approach, allowing for modulation of all characteristics of electromagnetic waves, paves the way to designing complex metasurfaces and meta-holograms with multiplexed functionalities, which may have applications in multichannel communication and data storage.

Keywords: Meta-holography, Polarization-frequency multiplexed, Phase-amplitude modulation

Qiu Wang, Xueqian Zhang, Prof. Eric Plum, Quan Xu, Minggui Wei, Yuehong Xu, Huifang Zhang, Yi Liao, Prof. Jianqiang Gu, Prof. Jiaguang Han, Prof. Weili Zhang**

Polarization and frequency multiplexed terahertz meta-holography